Journal Pre-proof

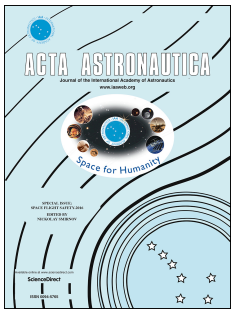

The Application of Tobler's Hiking Function in Data-Driven Traverse Modelling for Planetary Exploration

Arthur Goodwin, Megan Hammett, Myles Harris

PII: S0094-5765(24)00750-1

DOI: https://doi.org/10.1016/j.actaastro.2024.12.005

Reference: AA 10851

To appear in: *Acta Astronautica*

Received Date: 9 September 2024

Revised Date: 5 November 2024

Accepted Date: 5 December 2024

Please cite this article as: A. Goodwin, M. Hammett, M. Harris, The Application of Tobler's Hiking Function in Data-Driven Traverse Modelling for Planetary Exploration, *Acta Astronautica*, https://doi.org/10.1016/j.actaastro.2024.12.005.

The Application of Tobler's Hiking Function in Data-Driven Traverse Modelling for Planetary Exploration

Arthur Goodwin[1,2], Megan Hammett[1], Myles Harris[2,3]

[1]Department of Earth and Environmental Sciences, The University of Manchester, UK (arthur.goodwin@manchester.ac.uk)
[2]Space Health Research, London, UK
[3]Department of Risk and Disaster Reduction, UCL, UK

Abstract

Using data collected from the Meili-I analog crewed mission hosted on a remote Scottish island during August 2023, we analyze GNSS traverse tracks to assess walking velocity in relation to terrain slope. A series of data sampling tests to derive models using a generalized form of Tobler's Hiking Function indicates these models are only applicable to a similar resolution at which they were derived. Deriving walking velocity at 20-second intervals suggests a linear relationship between walking velocity and slope is useful for grid walking algorithms, but longer sampling intervals (>120 seconds) indicate a greater sensitivity to slope, likely recording long-period affects of exhaustion from prolonged ascending/descending of slopes. Findings are constrained by the limitations of environmental variables during the mission, including variable weather conditions and increasing familiarity with terrain. Applying calibrated hiking functions to grid walking algorithms (i.e., Dijkstra's algorithm) offers time-optimal paths useful for walk-back contingency planning but is unsuited for planning exploration geology traverses.

Key Words: Crewed Planetary Exploration, Analog, Hiking Function, Traverse Velocity, Fieldwork

1.0 Introduction

Crewed analog simulations provide a useful research methodology for investigating one or more aspects of future crewed spaceflight. Space Health Research organized Meili-I in the summer of 2023 as a two-week duration high-fidelity planetary exploration simulation approximating the remoteness, isolation, and scarcity of resources expected during upcoming planetary exploration. To assess the realistic possibility of field geology completed by humans on the surface of other planetary bodies (e.g., the Moon), analog fieldwork is necessary. Testing traverse planning strategies during *in-situ* exploration simulations has been a component for a number of analog missions [1–6].

For Meili-I, the crew were the major decision makers, planning traverses to key geological targets prior to deployment and tasked with navigation plus geological data collection during the simulations. Exploration field geology involves continued observation, interpretation, development and testing of hypotheses in the field, requiring complex decision-making [7–9]. Trying to integrate this geological methodology into the rigid constraints of astronaut traverses makes planning future astronaut traverses challenging. A key variable to consider is crew velocity over the planetary surface, which dictates the allocation between travel and activities during a time-limited traverse.

Tobler (ref.[10]) introduced an influential exponential equation to derive a relationship between the vector slope and walking velocity, which has become known as Tolber's Hiking Function (THF) — derived to estimate realistic time- or cost-distances between places. We classify "hiking function" as in Goodchild (ref [11]) referring to a general class of mathematical formula used to determine walking velocity considering the slope of the terrain. Hiking functions will most certainly be applicable for planning upcoming traverses for Artemis crewed landings on the Moon [12] but will need to consider different surface gravity.

THF is a vector function where the direction of travel over a terrain is necessary for determining the expected travel time. As in Goodchild (ref [11]) we define "slope" as a vector quantity evaluated in the direction of travel — specifically the tangent of the change in height experienced by the crew member for any given unit of horizontal distance covered. This differs from the gradient of the terrain, which is the absolute inclination typically recorded in Digital Terrain Models (DTM), considered as the tangent of the angle of a terrain surface to the horizontal.

A generalized form of THF can be written as:

$$w(x) = \alpha e^{-b|x+c|} \qquad \text{Equation 1}$$

Where w(x) represents the walking velocity in km/h, α is the maximum velocity, b is an exponent that modifies the velocity depending on slope, and c offsets the maximum walking velocity. Given that b controls the rate of velocity decline as slope increases, we will argue that this variable should be considered the "sensitivity" of walking velocity to slope. In Tobler's original function, α = 6 km/h, b = 3.5 and c = 0.05 such that the maximum walking velocity is achieved on a slight downslope [13,14]. The argument of the function is the change in elevation with change in distance, commonly given as $\partial h/\partial x$ — meaning a slope of 45° has a value of 1 [11].

Pace (hr/km) can be considered as the reciprocal of velocity, derived by inversing Equation 1 and expressed in a general form as [15]:

$$p(x) = \frac{1}{\alpha} e^{b|x+c|} \qquad \text{Equation 2}$$

Here, p(x) provides the time taken to cover any given (horizontal) distance. A complimentary function is vertical pace v(x), which provides the time needed to gain elevation (vertical displacement), and can be expressed as [15]:

$$v(x) = \frac{p(x)}{|x|} \qquad \text{Equation 3}$$

For a general THF, local minima in vertical pace v(x) occur for negative and positive values of x, which can be interpreted as the ideal slopes for losing or gaining elevation, respectively [15]. Local minima in v(x) indicate what degree of slope results in the fastest rate of elevation loss/gain.

The aim of this research was to use the passive geolocation datapoints collected during traverses during Meili-I to derive an accurate best-fit THF applicable for future traverse planning. Given that THF uses a slope vector input, it can be applied as an anisotropic cost function for accessibility analysis [16,17]. Here, cost function is defined in the context of network analysis as an attribute (e.g., slope, height gain, or time) used to model impedance, accumulated during traversal of a network. We derived data-driven THF models with variable sampling intervals, using the Meili-I mission data to assess the applicability of these models to grid walking, a popular method for route-planning [11,18,19]. An accurate model of crew walking velocity has implications for safety (including walk-back time [18]), minimizing crew workload, traverse planning to maximize time for data collection, and route-planning in otherwise topographically complex terrain.

2.0 Study Context

The study area used for the simulation was Lunga, an approximately 2 km^2 uninhabited Scottish island in the Firth of Lorn. With a maximum elevation of 98 m, the island is rugged comprising at least one paleocoastline terrace featuring a raised wavecut platform and cliffs. Underfoot was predominantly broken ground (complex terrain with a mixture of vegetation and rock creating obstacles) (Fig. 1) and crew members created their own trails rather than following previously trodden routes. Meili-I was a two-week mission completed during August of 2023. One smartphone used for data collection was carried between a crew of six fit and able-bodied people who walked with small “daybag” rucksacks. As such, velocity data presented (Supplementary Material 1) is for a group of six people who walked together and took turns carrying the smartphone.

The Meili-I crew navigated using Global Navigation Satellite System (GNSS) via the free mapping software Avenza Maps [20] hosted on a Motorola moto e30 android smartphone, using a georeferenced .pdf mapping product derived from the 1:25,000 ‘Explorer’ series Ordnance Survey map, which has 10 m topographic contours. Recorded crew velocity between geological localities is slowed by situations including: : (i) navigation of the complex terrain, and; (ii) review of geological features prior to deciding to stop and collect measurements. As such, velocity measurements represent a holistic spectrum of motion between hiking back to camp and slow, methodical exploration. This study did not consider a wide range of environmental variables that occurred during the two-week long study period which would have affected walking velocity, including: variable weather conditions, progressive exhaustion of crew members, and increasing familiarity with terrain aiding navigation.

3.0 Methods

Data processing was completed in Python v3.9, all code is available open-source on GitHub [21]. Initial GPS-tracking data was collected as part of the Meili-I mission recording circular traverses defined as containing a common start/end location. A total of 7 circular or almost-circular traverses were analyzed, selected between day five and day thirteen of the mission. Traverses vary in distance walked between 1.9 km and 7.4 km, constrained by the total length of the island of approximately 2 km laterally from the basecamp (Fig. 2). This distance is comparable to the 2 km radius of exploration expected for Artemis crewed landings —

defined as the maximum possible distance for a walking EVA [22,23]. As such, we treat the traverse data presented here for Meili-I in the context of a lunar analog. Data are provided in full in Supplementary Material 1.

Internal GNSS tracking with Motorola moto e30 android smartphones was used with only satellite fixes enabled. This technology was chosen due to budget restrictions and because smartphones for communication were already imbedded within the analog mission design. Avenza has the functionality to navigate upon multiple custom georeferenced .pdf basemaps, in additional to tracking capabilities. Default settings of low-accuracy location fixes (ignoring GNSS fixes with >32 m accuracy) were maintained, with a horizontal accuracy of 4.3 m [5.4/3.8 m] (median [Q3/Q1]; n=16941) and vertical accuracy of 2.8 m [4.2/1.9 m] (median [Q3/Q1]; n=16941) (Supplementary Material 2). This error is consistent with previous tests of similar smartphone technology [24]. Location fixes were recorded once two default thresholds had been overcome: (i) moving a horizontal distance >2 m, and; (ii) >2 seconds have passed. On average across the all analyzed traverses, this resulted in a location fix every 4.0 seconds [7.0/3.0 seconds] (median [Q3/Q1]; n=16934) (Supplementary Material 3). GNSS data recorded as a vector path was mapped onto a 5 m/pixel Ordnance Survey (OS) Terrain 5 DTM [25], which uses the British National Grid (BNG) grid reference system. The DTM is a raster grid of heightened points with a regular 5 m spacing and a typical vertical accuracy greater than 2 m Root Mean Squared Error (RMSE) — better than the elevation for GNSS location fixes recorded via the Avenza Maps mobile application.

To ensure continual and representative location fixes during the entirety of a circular traverse, the time-series data was downsampled via interpolation of the group mean. As this risked potential aliasing, a sensitivity test was run to assess the impact of time-series downsampling on derivation of a general hiking function (Fig. 3) — this sensitivity test investigates the effect of the spatial resolution of slope data. A filter of travelling a minimum distance of 5 m (the pixel size of the DEM raster) was used to threshold when the crew were walking — this data was used to derive general THF best-fits. The downsampling interpolation interval for location fixes was varied between 10 seconds and 300 seconds in 10 second steps (Supplementary Material 4). For each iteration, velocity and distance estimates were made using a straight-line distance from point-to-point with constant slope. A general THF was fitted to derive α, b, and c parameter values (Fig. 3). We note that straight-line distances between resampled geolocation points will fail to capture expected sinuosity in the actual path taken by crew members. Undulation in the terrain is also possible, indeed the DTM has a roughness value of 1.243±5.144 (mean±2σ; n=279189) over the 5 m/pix raster for the study area — calculated as the largest height difference of a central pixel and its surrounding cell of eight pixels [26].

Additionally, a cost analysis was developed applying Dijkstra's algorithm [27] weighted using an anisotropic THF model to effectively create a shortest-path tree — from which the most optimal route from a source node to specified target can be derived [28,29]. This cost-map is a raster representation of the study area where each cell contains a value representing how difficult it is to traverse that area. In our analysis, "cost" is the estimated time it takes to walk across the raster cell, calculated using a generalized THF. A shortest-path tree was derived from the starting coordinate to all other coordinates within the study area, using the 5 m/pixel OS Terrain 5 DTM raster grid. The algorithm was weighted using THF with parameters of α = 2.34, b = 1.00, and c = -0.01 (Modal B) to calculate the estimated travel time to adjacent

pixels weighed against slope. The search cell size for each pixel comprised the surrounding eight pixels, which limited the algorithm search to the eight cardinal (compass plus ordinal) directions. This is known to introduce erroneously longer travel time for non-cardinal bearings (which require a combination of cell moves) independent of raster cell size [11]. Change of direction at each pixel is also instantaneous. To ensure the cost analysis was realistic, slopes larger than 20° between any two grid pixels were made impassable.

4.0 Results

Across the downsampling interpolation interval sensitivity test for location fixes ranging from 10 to 300 seconds, we see variation in *α*, *b*, and *c* parameter values (Fig. 3). The *b* value — which effects the rate of velocity decline as slope increases (Equation 1) — stabilizes at approximately 2.96 for resampling intervals of 80–180 seconds, after which the value continues to increase. This stable *b* parameter represents a downsampling interval of 120 seconds and approximates ~50 m walking distance on flat terrain. At this downsampling interval, we derived a best-fit THF (R^2 = 0.175, no. points = 630) with parameter values of *α* = 1.58, *b* = 3.04, and *c* = 0.00, which equates to local minimal in the vertical pace (5.23) at slopes of ±18.26° (Equation 3). A symmetrical THF using values of *α* = 3.6, *b* = 3.5, and *c* = 0.00 suggested for off-path travel [10], provides excellent constraints for the maximum walking velocity on any given slope (Fig. 4a). Across all realistic downsampling intervals for the traverse tracks (Fig. 3) we see a lack of asymmetry (the *c* parameter approximates zero) meaning that uphill and downhill travel for a given slope takes the same amount of time. The R^2 value for downsampling intervals becomes stable with a value of ~1.7 for all windows of 60 seconds and longer, indicating these general THF share a similar goodness of fit and a consistent variability.

To assess the applicability of generalized THF models derived from differing downsampling intervals for grid walking, we compared the data collected for all seven traverses to two THF models — the first (Model A) using values of *α* = 1.58, *b* = 3.04, and *c* = 0.00 (R^2 = 0.175, no. points = 630) derived from the 120 second interpolation down-sampling interval (Fig. 4A; Equation 4), and the second (Model B) with values of *α* = 2.34, *b* = 1.00, and *c* = -0.01 (R^2 = 0.108, no. points = 2342) derived for a 20 second interval (Fig. 4B; Equation 5). Note that the geolocation fixes of the original data have a median spacing of 4.0 seconds (Supplementary Material 3). Model B differs in having a higher maximum walking velocity (*α* parameter) and a lower sensitivity to slope (higher *b* parameter) resulting in a near-linear change of walking velocity against slope which for the two near-symmetrical limbs (x-offset *c* = -0.01) can be estimated as straight line fit (R^2=0.999) with a gradient of ±0.035 (Fig. 4b). Note this best-fit gradient is significantly steeper than the velocity calculated using the cosine of slope — i.e., this line is not because linear map distances are used for the slope vector input or THF. This straight line fit results in local minimal in the vertical pace at slopes of ±45° (Equation 3).

Model A: $w(x) = 1.58e^{-3.04|x+0.00|}\ (km/h)$ Equation 4

Model B: $w(x) = 2.34e^{-1.00|x-0.01|}\ (km/h)$ Equation 5

Each of the seven traverses were rasterized to the 5 m/pixel OS DTM with each recorded time interval between GNSS location measurement, compared to estimates from the two models (Supplementary Material 5) (Fig. 5). Where the distance covered between GNSS location fixes was zero (e.g., for a rest break or activity station) the modelled time step instead used the measured time from the data. These values are excluded when comparing the error between the two models on a step-wise basis (Fig. 5b). Across all modelled traverses (Fig. 5c), 46% of the time steps were taken from the actual data due to distance travelled being less than the 5 m between adjacent pixels. As such we estimate that for a typical traverse, about 54% of the time (assuming no significant variation in time between location fixes) is spent walking between locations. The procedure for comparing Model A and Model B against recorded traverses (Fig. 5) was not used to assess goodness-of-fit to the data from which models were derived, but to evaluate the influence of sampling interval when applying these models to grid walking.

Depicting the Dijkstra's algorithm as a cost-map analysis for the whole study area (Fig. 6) we find it should take approximately 1.5 hours to cross the 2 km length of the study area — and thus a minimum of 3 hours for a circular traverse from the crew basecamp to the maximum extent of the study area and back. This time estimate assumes no stops. Indeed, during the Meili-I mission it took the crew approximately 3 hours to traverse the 2 km length of the island (6-hour circular journey).

5.0 Discussion

The sensitivity test at different downsampling interpolation intervals for location fixes highlights the importance of statistics when planning future planetary exploration traverses, notably if using straight line distances at scales up to ~100 m — in this case, the maximum distance covered if using the best-fit THF at the 300 second downsampling interval. Applying the general THF parameters from Model A (120-second interval) to the rasterized traverse (location fix every 4.0 seconds median) shows the model systematically overestimates walking velocity during relatively flat sections of the traverse (Fig. 5a). The model's higher sensitivity to slope (b-value) means it predicts travel times between location fixes ~5× slower than reality (Fig. 5b).On qualitative comparison, Model B (20-second interval) appears to be much more representative of travel-time (Fig. 5a) yet systematically underpredicts the time needed for traversing steeper slopes. Combining these insights with the sensitivity test (Fig. 3) effectively investigates how the spatial resolution of slope data effects model parameters. Indeed, we draw very similar conclusions to Pagneux et al. (ref. [30]): (i) the resolution of slope data (or slope data sampling) — compare Figure 4a and 4b —significantly impacts modelling outcomes for a general THF; (ii) a finer resolution increases similarity between the model and real data (Fig. 5), and; (iii) models are only applicable to a similar resolution from which they were derived. As such, we agree with Pagneux et al. (ref. [30]) that consistent spatial resolution is more important than cost functions for cost-path analysis.

At the time of writing, the highest resolution DEM of the lunar south pole region [31] has a resolution of 5 m/pix (the same used in this analog study) albeit with a typical data coverage of 10% meaning that 9 in 10 pixels are interpolated. This has implications for grid walking models weighted to slope — it can be expected that for any 50 m section of traverse only 5

m has a known elevation (with error). As such, applying path-finding algorithms to this resolution DEM when planning future lunar exploration may be ineffectual given a lack of granularity (level of detail represented in the data) and if longer averages are used, the appropriate hiking functions needs to be determined. So far, hiking functions applicable to lunar EVA has only been estimated for the Apollo era without a consistent spatial sampling window [12,18,32]. Uncertainty for future exploration to south polar regions of the Moon will need additional considerations including the influence of regolith bearing capacity on higher slopes [33], metabolic expenditure walking on more topographically complex terrain, and maneuverability of future EVA spacesuits. Given this uncertainty, a more general approach to deriving time estimates for a traverse exploring another planetary surface may provide more useful insight— for example cumulative elevation change and distance covered (as in ref. [1]). Applying Model B (20-second interval) to measured traverses we see a roughly linear relationship between traverse length and model error (error = 0.0031*traverse length + 82.34; no=5, R^2 = 0.44, units = m) which can be summarized as approximately accurate for a 6 km traverse with a cumulative +3.1% error for each additional kilometer (Fig. 5c). This consistent error suggests it can be corrected by adapting the hiking function, such as combining it with other pace functions (e.g., ref. [14]). Although at short 20-second intervals walking velocity varies linearly with slope (Fig. 4b) the cumulation of errors over longer periods (Fig. 5) shows small inclines in undulating terrain do not affect walking velocity as significantly as continued periods of ascending/descending. The higher-sensitivity to slope captured in the curve of Model A, and indeed the original THF [10], is likely a superposition of: (i) increased path sinuosity not captured in straight-line distance averages, and; (ii) a decrease in walking velocity due to the effort needed for periods of ascent/descent. As such, averaging THF parameters over longer periods of time results in different apparent behaviors. Indeed, we infer a lower maximum velocity in Model A compared to Model B is because of larger averaging intervals, resulting in actual routes becoming longer relative to the straight-line distance between sampling points. Ideally, a cost function for future crewed exploration — e.g., an upcoming Artemis lunar surface EVA — should consider an initial pixel-resolution equation of walking velocity with slope superposed with a second model for longer-interval running average considering prolonged ascent/descent as well as crew exhaustion. For the Moon, any function will have to consider differences in gait as a result of both lunar gravity and EVA suit design [34,35]. Although such a hiking function could be derived from the Meili-I mission, it is evident the detailed calibration necessary is at odds with the benefit of having a cosmopolitan “rule of thumb” equation that it applicable within dynamic and flexible mission planning.

This study could be improved by increased location accuracy, using more sophisticated GNSS receivers in combination with Real-Time Kinematic (RTK) correction services. However, location inaccuracy would still be expected for short dwell-times and moving instrumentation. For cost-map analysis applying models to a raster DEM, inferences are limited by both the accuracy and resolution of the dataset. Although a high-resolution (small pixel size) local DEM could be generated (e.g., by LIDAR) no comparable dataset for the Moon exists, hampering extraterrestrial application. We recommend future work towards running similar studies in higher-fidelity settings — e.g., more comparable lunar analog environments with crew members wearing restrictive EVA suits. Understanding the factors affecting mobility and thus walking velocity would improve hiking function models. As stated previously by Pingel (ref. [36]) using THF to weight path-finding algorithm generates time-optimal paths but fails as a descriptive model for how humans actually find routes through

topography, partly because slope imparts both a time and metabolic effort. Geological target allocation adds another variable to this. Typically, field geologists' endeavor to walk parallel to dip/orthogonal to the strike of the geological strata to investigate the widest variation in rock ages — which for this study area is E-W over the steepest sections of terrain. Both from human experience during the Meili-I mission and indeed by deriving a weighted cost-map analysis (Fig. 6) it is evident that N-S routes are optimal for traversing the study area. As such, Meili-I crew members were frequently not walking the most optimal routes. This behavior limits the application of grid-walking algorithms for route-planning future analog missions at this study area — and indeed for future lunar traverse featuring geological exploration. Least-cost routes derived for the study area from Figure 6 would all avoid the central N-S ridge of study area which is topographically complex but contains the richest geological exposures. However, generating cost-maps (Fig. 6) provides an important product for estimating walk back time [18,37] — the time for crew to return to the base in case of emergencies. Indeed, emergencies necessitate the most optimal/efficient routes back to safety and as such, we recommend hiking functions are most applicable in those scenarios rather than planetary exploration.

6.0 Conclusions

Using a data-driven approach to analyze crew traverses during the Meili-I mission, organized by Space Health Research for two weeks during August 2023, we analyzed GNSS tracks to determine models relating walking velocity to terrain slope. Application of THF indicates findings comparable to Pagneux et al. (ref. [30]), specifically that consistent spatial resolution is important when applying models to cost-path analysis. Comparison between two models — Model A; 20 second GNSS location fix average, and Model B; 120 second GNSS location fix average — indicates increasing sensitivity of crew velocity to slope when averaging over longer straight-line distances. Although this reflects the limitations of the methodology assumed in THF, it highlights the importance of defining and calibrating suitable models for future planetary exploration. Notably if planning future traverses in the lunar south polar region where the most recent DEM [31] has a 5 m/pixel resolution with 9 in 10 pixels being interpolated, the application of path-finding algorithms needs to be considered. Given the complexity of science targets during Meili-I and expected for upcoming Artemis missions, optimal route-finding via a calibrated hiking function may be more applicable to contingency planning for emergencies rather than exploration.

Acknowledgements

We would like to thank the entire Meili-I team (G. G., A. R., M. H., A. B., M. G., J. G.) for their commitment and support for this work. Thank you to the University of Manchester earth science department for borrowing geological equipment. This work was supported by the UK Science and Technology Facilities Council through a PhD studentship to A.G. (ST/V506886/1).

Declaration of competing interest

The authors declare that they have no known competing financial interests or personal relationships that could have appeared to influence the work reported in this paper.

Data availability

All data generated or analyzed during this study are included in this published article (and its supplementary information files).

References

[1] A. Kereszturi, Geologic field work on Mars: Distance and time issues during surface exploration, Acta Astronaut. 68 (2011) 1686–1701. https://doi.org/https://doi.org/10.1016/j.actaastro.2010.11.008.

[2] F. Hörz, G.E. Lofgren, J.E. Gruener, D.B. Eppler, J.A. Skinner, C.M. Fortezzo, J.S. Graf, W.J. Bluethmann, M.A. Seibert, E.R. Bell, The traverse planning process for D-RATS 2010, Acta Astronaut. 90 (2013) 254–267. https://doi.org/https://doi.org/10.1016/j.actaastro.2012.02.008.

[3] J.J. Marquez, M.J. Miller, T. Cohen, I. Deliz, D.S. Lees, J. Zheng, Y.J. Lee, B. Kanefsky, J. Norheim, M. Deans, S. Hillenius, Future Needs for Science-Driven Geospatial and Temporal Extravehicular Activity Planning and Execution, Astrobiology 19 (2019) 440–461. https://doi.org/10.1089/ast.2018.1838.

[4] J.L. Bresina, P.H. Morris, M.C. Deans, T.E. Cohen, D.S. Lees, Traverse Planning with Temporal-Spatial Constraints, in: Int. Conf. Autom. Plan. Sched. (ICAPS 2017), 2017.

[5] K. V Hodges, H.H. Schmitt, A new paradigm for advanced planetary field geology developed through analog experiments on Earth, in: W.B. Garry, J.E. Bleacher (Eds.), Analog. Planet. Explor., Geological Society of America, 2011: p. 0. https://doi.org/10.1130/2011.2483(02).

[6] J.M. Hurtado Jr, K. Young, J.E. Bleacher, W.B. Garry, J.W. Rice Jr, Field geologic observation and sample collection strategies for planetary surface exploration: Insights from the 2010 Desert RATS geologist crewmembers, Acta Astronaut. 90 (2013) 344–355.

[7] C.E. Carr, D.J. Newman, K. V Hodges, Geologic traverse planning for planetary EVA, in: 33rd Int. Conf. Environ. Syst., 2003: pp. 2003–2416.

[8] E.M. Riggs, C.C. Lieder, R. Balliet, Geologic Problem Solving in the Field: Analysis of Field Navigation and Mapping by Advanced Undergraduates, J. Geosci. Educ. 57 (2009) 48–63. https://doi.org/10.5408/1.3559525.

[9] C.G. Wilson, C.E. Bond, T.F. Shipley, How can geologic decision-making under uncertainty be improved?, Solid Earth 10 (2019) 1469–1488. https://doi.org/10.5194/se-10-1469-2019.

[10] W.R. Tobler, Three Presentations on Geographical Analysis and Modeling: Non-isotropic Geographic Modeling; Speculations on the Geometry of Geography; and Global Spatial Analysis, NCGIA, University of California, 1993. https://books.google.co.uk/books?id=nzL9OwAACAAJ.

[11] M.F. Goodchild, Beyond Tobler's Hiking Function, Geogr. Anal. 52 (2020) 558–569. https://doi.org/https://doi.org/10.1111/gean.12253.

[12] E. Peña-Asensio, J. Sutherland, P. Tripathi, K. Mason, A. Goodwin, V.T. Bickel, D.A. Kring, Automated astronaut traverses with minimum metabolic workload: Accessing permanently shadowed regions near the lunar south pole, Acta Astronaut. 214 (2024) 324–342. https://doi.org/https://doi.org/10.1016/j.actaastro.2023.10.010.

[13] W. Tobler, Three Presentations On Geographical Analysis And Modeling, (1999).

[14] J. Márquez-Pérez, I. Vallejo-Villalta, J.I. Álvarez-Francoso, Estimated travel time for walking trails in natural areas, Geogr. Tidsskr. J. Geogr. 117 (2017) 53–62. https://doi.org/10.1080/00167223.2017.1316212.

[15] E. Prisner, P. Sui, Hiking-time formulas: a review, Cartogr. Geogr. Inf. Sci. 50 (2023) 421–432. https://doi.org/10.1080/15230406.2023.2197625.

[16] C.D. Higgins, Hiking with Tobler: Tracking movement and calibrating a cost function for personalized 3D accessibility, Findings (2021).

[17] G. Alberti, movecost: An R package for calculating accumulated slope-dependent anisotropic cost-surfaces and least-cost paths, SoftwareX 10 (2019) 100331. https://doi.org/https://doi.org/10.1016/j.softx.2019.100331.

[18] C. Olthoff, EVA Walk-Back Limit Calculation Using the Virtual Spacesuit, 2018.

[19] Z. Magyari-Sáska, S. Dombay, Determining minimum hiking time using DEM, Geogr. Napocensis Anul 82 (2012) 124–129.

[20] Avenza, Avenza Maps, (n.d.). https://store.avenza.com/ (accessed August 22, 2024).

[21] A. Goodwin, ag00dwin/EVA_traversetime: hiking function best-fit and path-finding algorithm (v0.1.0), (2024). https://doi.org/10.5281/zenodo.13737869.

[22] E.J. Allender, C. Orgel, N. V Almeida, J. Cook, J.J. Ende, O. Kamps, S. Mazrouei, T.J. Slezak, A.-J. Soini, D.A. Kring, Traverses for the ISECG-GER design reference mission for humans on the lunar surface, Adv. Sp. Res. 63 (2019) 692–727. https://doi.org/https://doi.org/10.1016/j.asr.2018.08.032.

[23] N. Kumari, J.M. Bretzfelder, I. Ganesh, A. Lang, D.A. Kring, Surface conditions and resource accessibility at potential Artemis landing sites 007 and 011, Planet. Sci. J. 3 (2022) 224.

[24] P.A. Zandbergen, S.J. Barbeau, Positional Accuracy of Assisted GPS Data from High-Sensitivity GPS-enabled Mobile Phones, J. Navig. 64 (2011) 381–399. https://doi.org/DOI: 10.1017/S0373463311000051.

[25] Ordnance_Survey, OS Terrain 5, (2022). https://www.ordnancesurvey.co.uk/products/os-terrain-5#technical (accessed August 22, 2024).

[26] M.F.J. Wilson, B. O'Connell, C. Brown, J.C. Guinan, A.J. Grehan, Multiscale Terrain Analysis of Multibeam Bathymetry Data for Habitat Mapping on the Continental Slope, Mar. Geod. 30 (2007) 3–35. https://doi.org/10.1080/01490410701295962.

[27] E.W. Dijkstra, A Note on Two Problems in Connexion with Graphs, in: Edsger Wybe Dijkstra His Life,Work, Leg., 1st ed., Association for Computing Machinery, New York, NY, USA, 2022: pp. 287–290. https://doi.org/10.1145/3544585.3544600.

[28] H. Antikainen, Using the Hierarchical Pathfinding A* Algorithm in GIS to Find Paths through Rasters with Nonuniform Traversal Cost, ISPRS Int. J. Geo-Information 2 (2013) 996–1014. https://doi.org/10.3390/ijgi2040996.

[29] J.S.B. Mitchell, Shortest paths and networks, in: Handb. Discret. Comput. Geom., Chapman and Hall/CRC, 2017: pp. 811–848.

[30] E. Pagneux, E. Sturludóttir, R. Ólafsdóttir, Modelling of recreational trails in mountainous areas: An analysis of sensitivity to slope data resolution, Appl. Geogr. 160 (2023) 103112. https://doi.org/https://doi.org/10.1016/j.apgeog.2023.103112.

[31] M.K. Barker, E. Mazarico, G.A. Neumann, D.E. Smith, M.T. Zuber, J.W. Head, Improved LOLA elevation maps for south pole landing sites: Error estimates and their impact on illumination conditions, Planet. Space Sci. 203 (2021) 105119. https://doi.org/https://doi.org/10.1016/j.pss.2020.105119.

[32] R.S. Johnston, L.F. Dietlein, C.A. Berry, Biomedical results of Apollo, Scientific and Technical Information Office, National Aeronautics and Space …, 1975.

[33] H.M. Sargeant, V.T. Bickel, C.I. Honniball, S.N. Martinez, A. Rogaski, S.K. Bell, E.C. Czaplinski, B.E. Farrant, E.M. Harrington, G.D. Tolometti, D.A. Kring, Using Boulder Tracks as a Tool to Understand the Bearing Capacity of Permanently Shadowed Regions of the Moon, J. Geophys. Res. Planets 125 (2020) e2019JE006157. https://doi.org/https://doi.org/10.1029/2019JE006157.

[34] C.E. Carr, J. McGee, The Apollo Number: Space Suits, Self-Support, and the Walk-Run Transition, PLoS One 4 (2009) e6614. https://doi.org/10.1371/journal.pone.0006614.

[35] K.J. Kim, A. Baughman, P. Estep, E. Rivas, M. Young, K. Marshall-Goebel, A. Abercromby, J. Somers, Uneven terrain affects metabolic cost and gait in simulated complex lunar surfaces, Physiol. Meas. 44 (2023) 104001. https://doi.org/10.1088/1361-6579/acf993.

[36] T.J. Pingel, Modeling Slope as a Contributor to Route Selection in Mountainous

Areas, Cartogr. Geogr. Inf. Sci. 37 (2010) 137–148. https://doi.org/10.1559/152304010791232163.

[37] J.R. Norcross, L.R. Lee, K.G. Clowers, R.M. Morency, L. Desantis, J.K. De Witt, J.A. Jones, J.R. Vos, M.L. Gernhardt, Feasibility of performing a suited 10-km ambulation on the moon-final report of the EVA walkback test (EWT), Johnson Sp. Center, Houston, TX 48 (2009).

Fig. 1. Photograph showing the terrain and topography of the Scottish island used as a study area for the duration of the Meili-I two-week mission.

Fig. 2. A topographic map of the study area. The basemap is a 1:25,000 'Explorer' series Ordnance Survey map; this was rescaled to 1:10,000 and printed as A4 size for navigation during the mission. Annotations: a simplified summary of the geology is provided with a N/S trending uncomfortable contact marked, separating the island into east and west areas — inset on the bottom left shows rock bed orientation measurement and the means are plotted as symbols on the map; the "basecamp" used as the beginning and end of circular traverses is marked with a star; a 2 km radial distance (R) was the furthest extend travelled by analog crew members; the red line is the recorded GNSS track of traverse route on the ninth day of the mission. Geological localities visited during this day are marked by open black triangles.

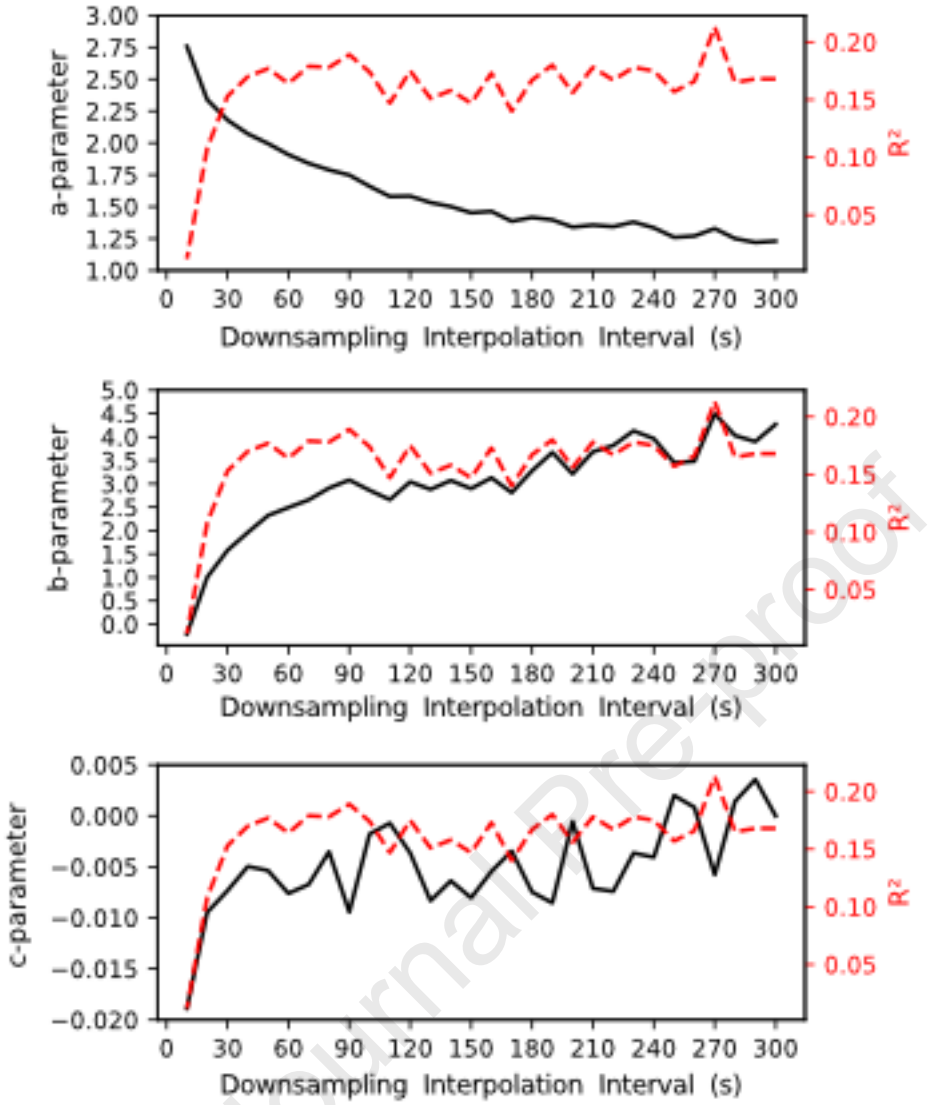

Fig. 3. Results on the sensitivity test to assess the time-series downsampling of GNSS location fixes between a 10 second and 300 second interpolation interval. The average GNSS location fix was calculated and straight-line distances used to derive the three parameters for a generalized Tobler's Hiking Function (THF) best-fit (see Equation 1).

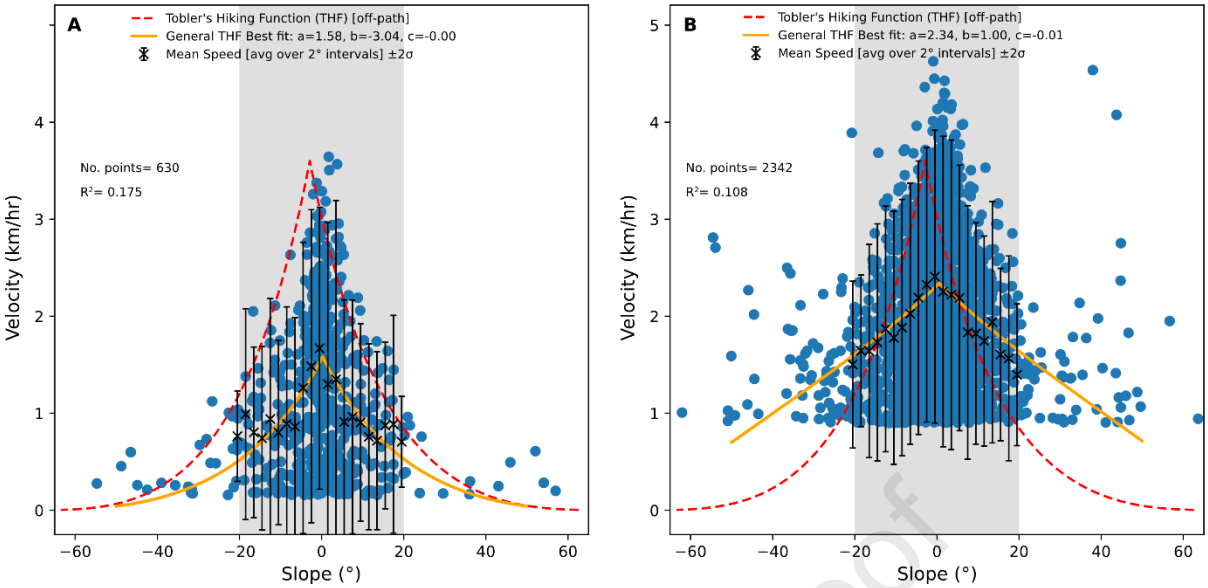

Fig. 4. Plots of walking velocity against slope for two generalized THF fits: (A) Model A derived from a 120 second downsampling interpolation interval (Equation 4), and; (B) Model B derived from a 20 second downsampling interpolation interval (Equation 5). The dashed line shows the original THF for off-path travel. The gray zone shows the range of positive and negative slope values (±20°) over which the THF best-fit was estimated via a least-squares approach. Additionally, GNSS fixes were binned in 2° intervals and the mean ±2σ are plotted for each bin. Slope values larger than ±20° are likely due to GNSS location errors.

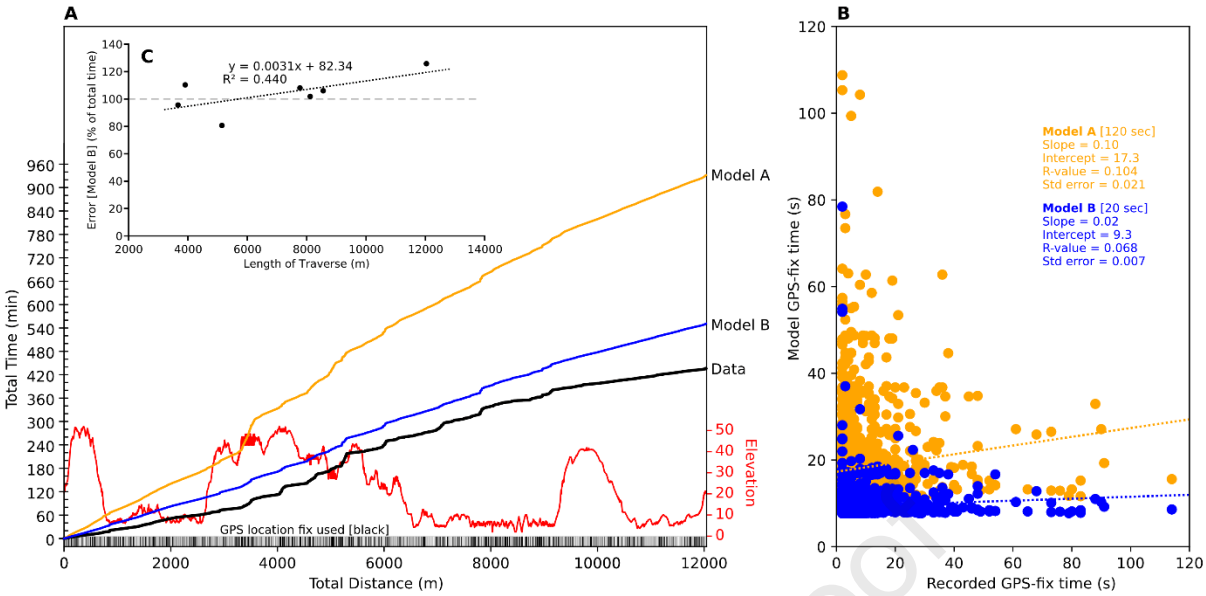

Fig. 5. Summary of traverse nine (shown in Fig. 2) showing: (A) the topographic height profile against distance (red) and the three profiles of cumulative distance versus time for the traverse, (black = data; orange = Model A; blue = Model B) — note that model profiles are only for geolocation fixes where the distance travelled was more than 5 m, depicted graphically at the bottom of plot where black represents modelled datapoints; (B) plot of recorded time between GNSS location fixes and modelled time derived from generalized functions (orange = Model A; blue = Model B), lines of best fit for both models show deviation from a gradient of 1 which would represent a perfect match between data and the models; (C) Plot of cumulative distance of each traverse against the percentage error between the actual time and modelled time (Model B) at the end of the traverse, a linear line of best fit is for all traverses.

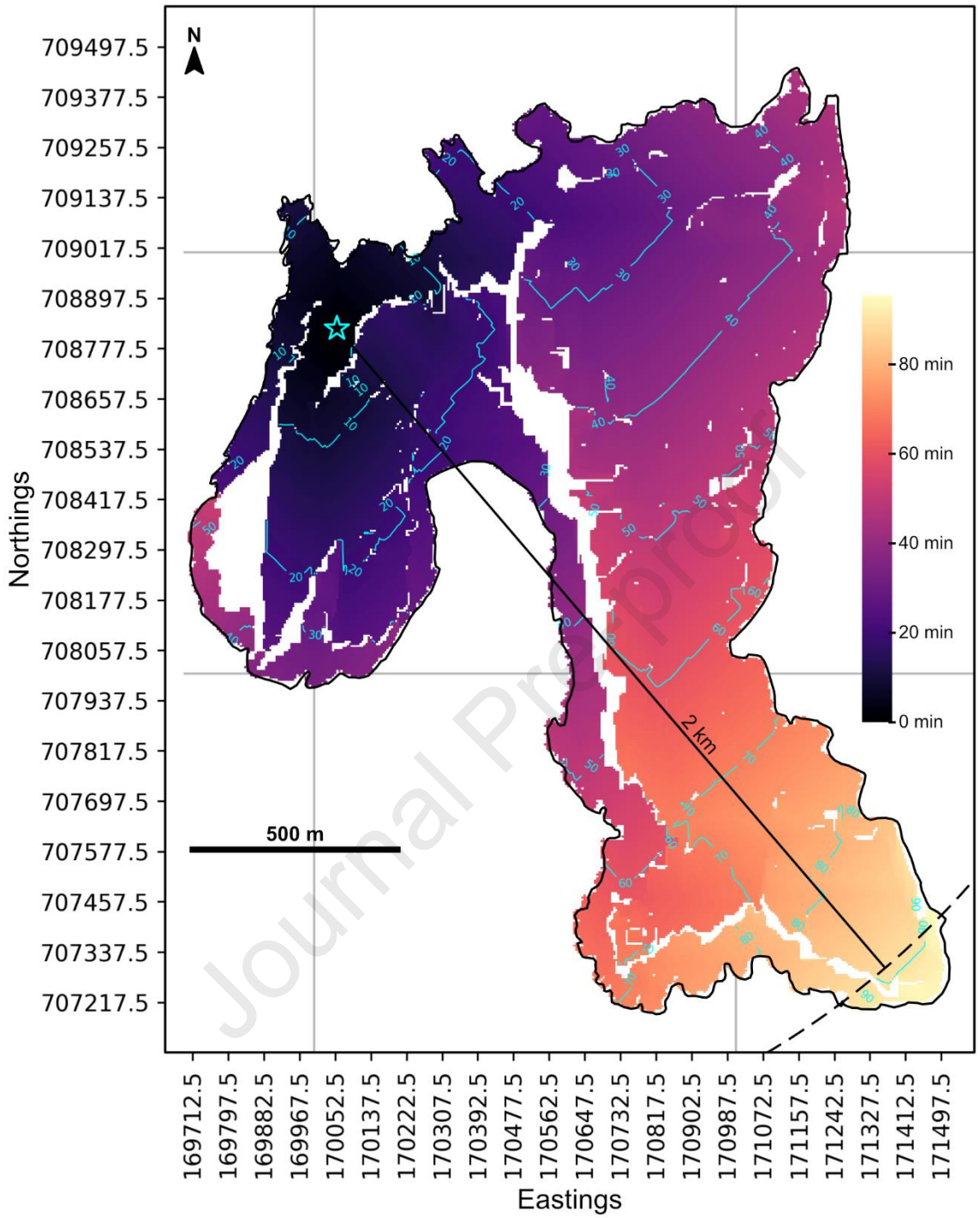

Fig. 6. Cost-map analysis plot calculated using a Dijkstra's algorithm weighted against slope (Model B, Equation 5) initiating at the crew basecamp labelled to every pixel of the 5 m/pixel OS Terrain 5 DTM raster grid. The colored heatmap depicts the time estimate for the most optimal path from the pixel back to the starting location (basecamp, blue star). Time contours constrain distance with the same estimated time for optimal paths in 10-minute intervals. The extent of the exploration area on the island is shown in black (mean high water springs; MWHS). Areas in white are inaccessible, either because they are beyond the coastline in the sea or the ground has a gradient greater than 20°, meaning crew would need to either climb or scramble, rather than walk.

Supplementary Information 1. Spreadsheets exported from the Avenza maps mobile application providing the GNSS location fixes for the seven recorded traverse.

Supplementary Information 2. Boxplots of the location accuracy of (A) spatial XY error and (B) elevation Z error, for every GNSS location fix across all seven traverses.

Supplementary Information 3. Variation in periodicity of GNSS location fix showing: (A) histogram of time periods between GNSS location fixes, and; (B) boxplot of time periods between GNSS location fixes — including magnified view.

Supplementary Information 4. Results on the sensitivity test to assess the time-series downsampling of GNSS location fixes between 10 second and 300 seconds, with a best-fit generalized Tobler's Hiking Function (THF) for each 10-second interval. See Figure 4 for more detail regarding individual plots, and Figure 3 for a summary of the generalized THF parameters resulting from each fit.

Supplementary Information 5. Summary of each traverse (as in Figure 5) showing: (A) the topographic height profile against distance (red) and the three profiles of distance versus time for the travers (black = data, orange = Model A, blue = Model B) — modelled profiles are only for geolocation fixes where the distance travelled more than 5 m, depicted graphically at the bottom plot where black represents modelled datapoints; (B) plot of recorded time between GNSS location fixes and modelled time derived from generalized functions (orange = Model A; blue = Model B), lines of best fit for both models show deviation from a gradient of 1 which would represent a perfect match between data and the models

Highlights

- Tracking of crew during a mission simulation shows how walking velocity changes with slope
- Data sampling tests show hiking functions only apply to a resolution similar to their derivation
- Sensitivity of velocity to slope increases when averaging over longer straight line distances
- Paths from grid walking algorithms are suited to contingency planning rather than exploration

Declaration of interests

☒ The authors declare that they have no known competing financial interests or personal relationships that could have appeared to influence the work reported in this paper.

☐ The author is an Editorial Board Member/Editor-in-Chief/Associate Editor/Guest Editor for *[Journal name]* and was not involved in the editorial review or the decision to publish this article.

☐ The authors declare the following financial interests/personal relationships which may be considered as potential competing interests: